# Improved efficiency of the biological pump as a trigger for the Late Ordovician glaciation

Jiaheng Shen<sup>1,2\*</sup>, Ann Pearson<sup>1\*</sup>, Gregory A. Henkes<sup>1,3</sup>, Yi Ge Zhang<sup>1,4</sup>, Kefan Chen<sup>5</sup>, Dandan Li<sup>5</sup>, Scott D. Wankel<sup>1</sup>, Stanley C. Finney<sup>7</sup> and Yanan Shen<sup>1</sup>

The first of the 'Big Five' Phanerozoic mass extinctions occurred in tandem with an episode of glaciation during the Hirnantian Age of the Late Ordovician. The mechanism or change in the carbon cycle that promoted this glaciation, thereby resulting in the extinction, is still debated. Here we report new, coupled nitrogen isotope analyses of bulk sediments and chlorophyll degradation products (porphyrins) from the Vinini Creek section (Vinini Formation, Nevada, USA) to show that eukaryotes increasingly dominated marine export production in the lead-up to the Hirnantian extinction. We then use these findings to evaluate changes in the carbon cycle by incorporating them into a biogeochemical model in which production is increased in response to an elevated phosphorus inventory, potentially caused by enhanced continental weathering in response to the activity of land plants and/or an episode of volcanism. The results suggest that expanded eukaryotic algal production may have increased the community average cell size, leading to higher export efficiency during the Late Katian. The coincidence of this community shift with a large-scale marine transgression increased organic carbon burial, drawing down CO<sub>2</sub> and triggering the Hirnantian glaciation. This episode may mark an early Palaeozoic strengthening of the biological pump, which, for a short while, may have made eukaryotic algae indirect killers.

t is estimated that 26% of families and 49% of genera of marine biota were lost during the Hirnantian extinction<sup>1</sup>, possibly due to glacially-driven reduction in shallow water habitats<sup>2-4</sup>. This climate event is notable for following a period of relatively high atmospheric CO<sub>2</sub> (refs <sup>5-8</sup>). Hypotheses for understanding the unique combination of mass extinction with glaciation include changes in the balance of the carbon cycle<sup>3</sup>, enhanced silicate weathering9, and increased planetary albedo caused by high rates of volcanism10; however, none of these mechanisms can fully explain the observations. Perturbation of the carbon cycle is indicated by the widespread Hirnantian Isotope Carbon Excursion (HICE)3,11. In some interpretations, enhanced organic carbon burial occurred simultaneously with the HICE episodes and the Hirnantian glaciation; that is, the marine carbon isotope mass balance was directly linked with organic burial<sup>3,12,13</sup>. However, there is an alternative, model-based interpretation of the record, which finds that the positive carbonate δ<sup>13</sup>C excursion observed in the early Hirnantian is the expected response to increased weathering of carbonate platforms during the resulting glacioeustatic sea-level lowstand9. This latter scenario is consistent with observations that deposition of organic-rich shales in the Hirnantian is rather restricted, occurring in limited spatial and temporal patterns, with sedimentation instead favouring grey shelly limestone<sup>11</sup>. Decreased anoxia associated with glacially-synchronous cooling and deep ocean ventilation14 may have limited organic matter preservation, and a high rate of organic burial may not have persisted long into the Hirnantian. Such a scenario implies that the mechanisms to explain enhanced organic carbon deposition leading up to the extreme and abrupt climate change of the Late Ordovician must have begun earlier, in the Katian.

Bulk sedimentary nitrogen isotopic analyses ( $\delta^{15}N_{TN}$ , total nitrogen) provide insight into the marine nitrogen cycle at this time<sup>11,14,15</sup> (Supplementary Fig. 1). Anoxic marine settings during the late Katian promoted denitrification, resulting in loss of fixed nitrogen. Low values of  $\delta^{15}N_{TN}$  are thought to reflect replenishment of this nitrogen and therefore a major contribution of N-fixing cyanobacteria to the marine nitrogen budget. The importance of bacterial inputs during the Late Ordovician is supported by high hopane/ sterane (H/St) ratios<sup>16</sup>, a qualitative rather than quantitative indicator of community composition, and not necessarily derived from photosynthetic taxa<sup>17</sup>. However, such arguments are distinct from information specifically on export production and carbon burial, which can be dominated by eukaryotic phytoplankton even under conditions of low  $\delta^{15}N_{TN}$  (ref. <sup>18</sup>). Here we focus on quantitative estimates of phytoplankton community structure and export efficiency to determine the resulting effects on the global carbon cycle.

# Nitrogen isotopic records of sediments and porphyrins

In sediments from Vinini Creek, coeval bulk organic matter and vanadyl (VO) porphyrins (Supplementary Table 1) show isotopic trends and patterns that are different for nitrogen when compared to carbon (Fig. 1; Supplementary Table 2). A positive excursion in the  $^{13}$ C content of organic matter ( $\delta^{13}$ C $_{\rm org}$ ) of  $\sim\!2\%$  is coincident with the immediate transition from the Katian to the Hirnantian (Fig. 1b). However, a better comparison may be between the more similar limestone-rich facies of the earlier *Dicellograptus ornatus* zone (mean  $\delta^{13}$ C $_{\rm org}\approx-30.5\%$ ) and the Hirnantian (mean  $\delta^{13}$ C $_{\rm org}\approx-29.5\%$ ), which, if  $\delta^{13}$ C values of bulk organic and inorganic carbon are shifting in parallel, is equivalent to a+1% excursion in  $\delta^{13}$ C values of carbonates  $^{11,19}$ , or a modest effect on the total carbon

<sup>1</sup>Department of Earth and Planetary Sciences, Harvard University, Cambridge, MA, USA. <sup>2</sup>Institute of Geology and Geophysics, Chinese Academy of Sciences, Beijing, China. <sup>3</sup>Department of Geosciences, Stony Brook University, Stony Brook, NY, USA. <sup>4</sup>Department of Oceanography, Texas A&M University, College Station, TX, USA. <sup>5</sup>School of Earth and Space Sciences, University of Science and Technology of China, Hefei, China. <sup>6</sup>Department of Marine Chemistry and Geochemistry, Woods Hole Oceanographic Institution, Woods Hole, MA, USA. <sup>7</sup>Department of Geological Sciences, California State University, Long Beach, CA, USA. \*e-mail: jiahengshen@fas.harvard.edu; pearson@eps.harvard.edu

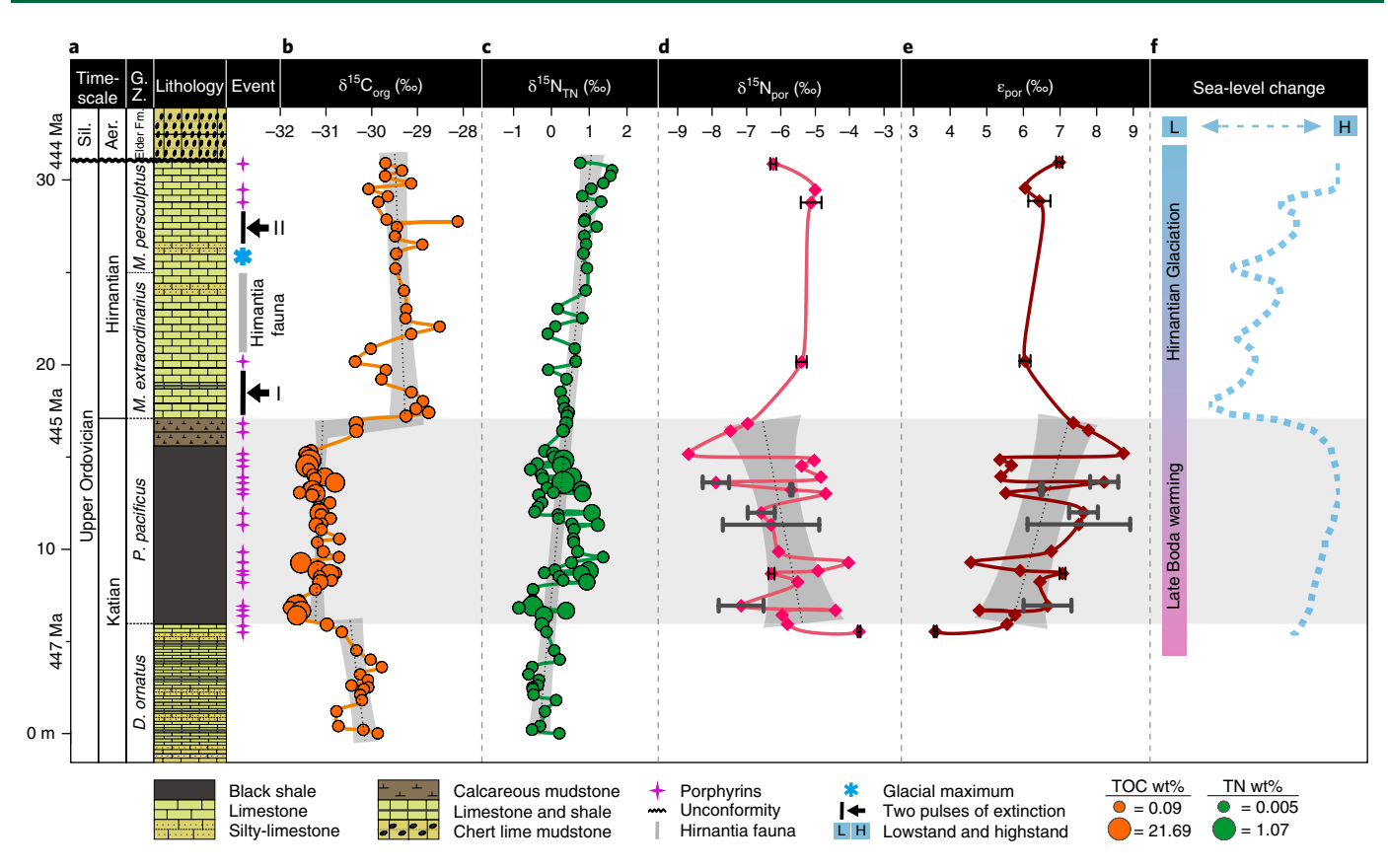


**Fig. 1** Late Ordovician chronology, stable isotope, lipid biomarker, and sea-level stratigraphic records from Vinini Creek, Nevada, USA. **a**, Litho- and biostratigraphy, lithology, palaeoclimate and bioevents. **b,c**, Values of  $\delta^{13}C_{org}$  and  $\delta^{15}N_{TN}$  together with %TOC and %TN (orange and green circles, size of symbol proportional to %). **d**, Porphyrin nitrogen isotopic compositions ( $\delta^{15}N_{por}$  pink diamonds). **e**, The isotopic difference between bulk sediment and porphyrin ( $\epsilon_{por}$  dark red diamonds). **f**, Sea-level curve from refs <sup>42,43</sup>. Black dashed lines and grey intervals on isotopic data represent linear fit and 95% confident interval, respectively. Linear regressions and 95% CI were calculated for all data in GraphPad Prism V. 7.0. Black arrows represent two phases of mass extinction. G.Z., graptolite zones; Sil., Silurian; Aer., Aeronian; Elder Fm., Silurian Elder Formation. All error bars reflect 1 $\sigma$  precision. The thin black error bars represent analytical precision. The wide black error bars represent full-process replicates. Data in Supplementary Table 2.

cycle. The more negative  $\delta^{\scriptscriptstyle 13}C_{\scriptscriptstyle org}$  values from the organic-rich black shale of the Katian Paraorthograptus pacificus zone may reflect a change in local organic matter type, indicating a turnover in the phytoplankton community and/or a change in factors affecting carbon uptake and subsequent diagenesis. In contrast to these facies-related carbon differences, the  $\delta^{15}N_{TN}$  profile shows a small and consistently positive trend throughout both the Katian and the Hirnantian (Fig. 1c). It is unlikely that our  $\delta^{15}N_{TN}$  record has been significantly altered by diagenesis, as the sediments are organic-rich, of low maturity<sup>20,21</sup>, and agree well with other Late Ordovician records<sup>11,14,15</sup> (Supplementary Figs. 1-4). A strong positive correlation between TN and TOC and zero intercept suggests little or no addition of detrital ammonium (Supplementary Fig. 2). Simultaneously, the porphyrin  $\delta$  $^{15}$ N ( $\delta^{15}$ N<sub>nor</sub>) value decreases by ~4‰ throughout the Katian *P. pacifi*cus zone and reaches its most negative value (approximately -8.5%) near the termination of black shale deposition (Fig. 1d). This is followed by a partial rebound in  $\delta^{15}N_{por}$  values during the Hirnantian.

# The $\varepsilon_{por}$ proxy for eukaryotic versus cyanobacterial burial

The isotopic difference between porphyrins and bulk nitrogen,  $\epsilon_{por}$  ( $\epsilon_{por=}\delta^{15}N_{TN}-\delta^{15}N_{por}$ ), can be used to estimate the fractional export production of eukaryotes and cyanobacteria  $^{18}$ . The approach derives from experiments that examined the offset between chloropigments and corresponding biomass  $\delta^{15}N$  values, indicating that  $\epsilon_{por}$  varies taxonomically  $^{22}$ . Average chloropigments have  $\epsilon_{por}=0\pm2\%$  for marine cyanobacteria,  $6\pm1\%$  for anoxygenic

(sulfur-oxidizing) photosynthetic bacteria, and  $5\pm2\%$  for eukary-otic algae<sup>22–24</sup>. Contributions from anoxygenic photosynthesis are not likely to contribute a major fraction of the total porphyrins, as there is neither evidence for euxinia at Vinini Creek<sup>25</sup>, nor for okenone, the characteristic carotenoid of purple sulfur bacteria, in the Late Ordovician<sup>26</sup>.

Values of  $\varepsilon_{por}$  at Vinini Creek average  $6.3 \pm 1.2\%$  (Fig. 1e). Due to diagenetic offsets that produce 15N depletions in VO porphyrins relative to other chloropigments<sup>27</sup>, the average value of  $\varepsilon_{por}$  for our Vinini Creek samples is evaluated on an endmember scale of 2.5-7.5% (100% cyanobacterial to 100% eukaryotic) rather than 0-5‰ to account for these diagenetic offsets. The significant ambiguity in this diagenetic isotope shift contributes uncertainty to our estimates of the absolute percentage of eukaryotes, but it will not change the relative magnitude of the estimated community shift because the scale range remains 5‰. More work is needed to better constrain the diagenetic and isotopic fates of porphyrins (discussion in the section 'Consideration of porphyrin diagenesis' in Methods; Supplementary Fig. 9). A minimum  $\varepsilon_{por}$  value of ~3% is observed in the uppermost part of the D. ornatus zone, while a pronounced trend of increasing  $\varepsilon_{por}$  is observed throughout the *P. pacificus* zone. The absolute values and temporal evolution in  $\varepsilon_{por}$  suggest that eukaryotes increasingly dominated export production throughout the Katian, expanding from ~20% to effectively account for ~100% of export by the end of the age. With the glacial onset, values of  $\varepsilon_{por}$  descend back to ~5%, perhaps indicating partial re-expansion ARTICLES NATURE GEOSCIENCE

of cyanobacteria. This turning point at the onset of the Hirnantian glaciation, specifically a contraction of eukaryotic algae, is consistent with microfossil analyses of acritarch assemblages<sup>28</sup>.

## Increased biological pump during the Late Ordovician

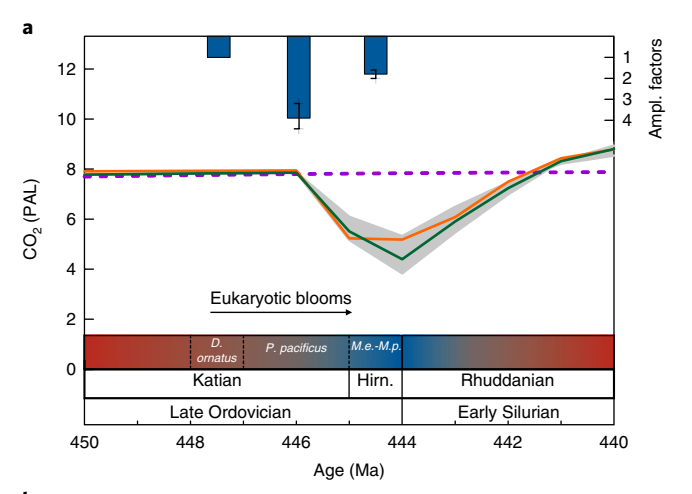
An interpretation of increased eukaryotic export and burial in the Katian contrasts with previous studies that invoked a high apparent abundance of cyanobacteria before the Hirnantian glaciation<sup>11,14-16</sup>. Lenton et al.<sup>29</sup> proposed that marine productivity in the Late Ordovician was enhanced by phosphorus weathering from continents. However, an increase in surface water productivity is not necessarily equivalent to greater biological export<sup>30-32</sup>. Whereas large phytoplankton cells sink passively and quickly, picoplankton, including cyanobacteria, are characterized by slow sinking and correspondingly high relative rates of remineralization. Smaller cells are easily entrained in resuspension loops, whereas larger cells have more chances to escape these loops and sink<sup>33</sup>, leading to significantly amplified export production as the dominance of large-sized phytoplankton increases<sup>34</sup>. Thus, community structure—in addition to productivity—strongly influences export, favouring the sedimentation of larger cells and the sequestration of more CO<sub>2</sub> as the fractional number of eukaryotes increases<sup>32,35</sup>.

Simultaneous with the inferred eukaryotic expansion, the preglacial late Boda warming and marine transgression  $^{11,36}$  (Fig. 1f) would have created greater accommodation space for bulk sediment accumulation. Although the magnitude of this increase is not well understood for the Late Ordovician, a similar sea-level rise during the Cretaceous was estimated to increase organic carbon burial by 30% (ref.  $^{37}$ ). The late Katian may therefore reflect the first convergence of multiple, synergistic factors that together triggered sufficient  ${\rm CO}_2$  decline to promote glaciation: enhanced phosphorus weathering, increased eukaryotic algal dominance, and a major transgression.

To systematically quantify Late Ordovician organic carbon burial, we compiled a database for the D. ornatus, P. pacificus and Hirnantian intervals for all available sections (Supplementary Fig. 5 and Supplementary Table 3). Normalized to the *D. ornatus* zone, the observed marine organic carbon burial flux appears to have been higher by a factor of 3.9 (min: 3.2 and max: 4.4) during the P. pacificus zone and by a factor of 1.8 (min: 1.6 and max: 2.0) during the Hirnantian (Supplementary Fig. 6), indicating that the increase in carbon burial occurred prior to glacial onset. Although the sedimentation database (Supplementary Table 3) certainly must reflect locations that had different degrees of upwelling-driven production, all sites except one show enhancement in the Late Ordovician. Because the  $\delta^{15}N_{TN}$  records from Vinini Creek are well correlated with other available Late Ordovician records from other palaeocontinents (Supplementary Fig. 1), the observed biogeochemical trends are likely to be global, and Vinini Creek may generally represent productive upwelling zones during the Late Ordovician. Since coastal upwelling regions, which support high export production, are critical determinants of global carbon and nitrogen cycles<sup>38</sup>, the data reported here can be generalized—especially because, for modelling purposes, they are averaged with the rest of the Late Ordovician sedimentation database (Supplementary Table 3) and are not the sole factor driving our results.

# Biological pump effects on organic carbon burial

Given the hypothesized increase to the efficiency of the Katian biological pump we evaluate the expected CO<sub>2</sub> decrease using an adapted Carbon Oxygen Phosphorus Sulphur Evolution (COPSE) model<sup>29,39</sup> (see Methods). A baseline run, with no change in production or burial, a constant global average temperature of 17 °C, and eight times present atmospheric level (8 PAL) CO<sub>2</sub>, yielded background conditions consistent with prior model implementations and proxy constraints<sup>7,8,29</sup> (dashed lines, Fig. 2). Directly forcing



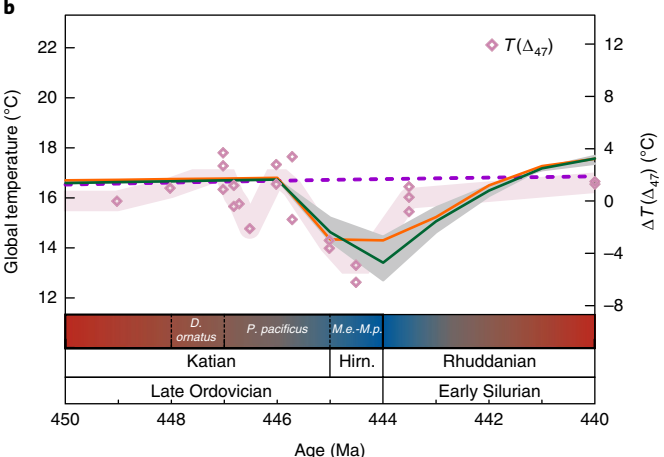


Fig. 2 | Model predictions. a,b, COPSE model results of Late Ordovician variation in atmospheric CO<sub>2</sub> concentration (a) and global temperature (b). Baseline with geological and biological forcing from ref. <sup>29</sup> (dashed lines); simulation of geological records of transient enhancement of marine organic carbon burial (green lines); prediction by introducing enhancement of phosphorus weathering, sea-level rise and phytoplankton community changes (orange lines). Shaded grey areas represent the ranges of atmospheric CO<sub>2</sub> and global temperature, where the lower and upper limits are predicted by directly forcing organic burial with maximum and minimum from the flux database, respectively (see Methods). Blue bars represent the amplification factors of marine organic carbon burial during the P. pacificus zone and Hirnantian. Error bars represent the maximum and minimum amplification values. Pink diamonds and trendline are the change in  $\Delta_{47}$ -derived near-surface ocean temperature from wellpreserved brachiopods in ref. <sup>2</sup>. Ampl., amplification; M.e., Metabolograptus extraordinarius; M.p., Metabolograptus persculptus.

burial by the flux database amplification factors of 3.9 for the latest Katian and 1.8 for the Hirnantian (green lines, Fig. 2) resulted in a  $\rm CO_2$  decrease to ~5 PAL at 445 million years ago (Ma) and a continued decline to ~4 PAL at 444 Ma (Fig. 2a). This is consistent with the consensus that the glaciation expanded, reaching maximum ice extent in the Early–Middle Hirnantian<sup>11</sup>. These changes translate in the model to a global cooling to ~14 °C at 445 Ma and ~13 °C at 444 Ma (Fig. 2b), in agreement with the apparent cooling trend in the Hirnantian reconstructed from carbonate clumped isotope thermometry, but with a smaller magnitude (3–4 °C global cooling predicted in COPSE model runs versus an up to 7 °C drop in tropical sea-surface temperatures from proxy data²). The difference between model and observational data may be due to a greater climate sensitivity in the Ordovician<sup>40</sup>, possibly in response to differences in

palaeogeography; the COPSE model assumes the present-day sensitivity of  $3\,^{\circ}\text{C}$  per CO<sub>2</sub> doubling. The model results demonstrate that the increased organic burial flux before the Hirnantian could have resulted in rapid cooling of the global climate.

To examine how this burial amplification was promoted, we subsequently removed the constraint of directly forced burial, instead modelling it using two new variables-phytoplankton export efficiency and sea-level change—in combination with phosphorus forcing as implemented by Lenton et al.<sup>29</sup>. Phytoplankton export efficiency was implemented by dividing the community into small (cyanobacterial) and large (eukaryotic) fractions based on  $\varepsilon_{por}$  data, and then varying the export probability for each pool according to relative cell sizes (Supplementary Fig. 10). The export efficiency terms, plus sea-level and phosphorus variables, were then optimized to fit the observed organic burial record (sensitivity analyses; Supplementary Fig. 8 and Supplementary Tables 4-5). A solution in which accommodation space is increased by 30% to account for the transgression<sup>37</sup>, phosphorus weathering is amplified by a factor of approximately two (instead of the factor of three used in earlier simulations<sup>29</sup>), and burial efficiency of the eukaryotic fraction of export production is increased by a factor of four (consistent with doubling the average cell size according to Stokes' Law, assuming that burial efficiency scales with velocity, a conservative estimate<sup>41</sup>), adequately simulates the glacial scenario (orange lines, Fig. 2). All three variables appear to play significant roles in the increased organic burial flux; and importantly, together they alleviate some of the need to greatly enhance continental weathering (that is, they reduce the phosphorus amplification) at a time when the expansion of terrestrial plant biota—which changed continental weathering regimes—was still in its relative infancy. Nutrient-driven expansion of larger-celled eukaryotic production in association with a marine transgression was a calamitous combination that promoted glaciation and, ultimately, shallow-water extinctions.

#### Methods

Methods, including statements of data availability and any associated accession codes and references, are available at https://doi.org/10.1038/s41561-018-0141-5.

Received: 19 December 2017; Accepted: 25 April 2018; Published online: 11 June 2018

#### References

- Sepkoski, J. J. in Global Events and Event Stratigraphy in the Phanerozoic: Results of the International Interdisciplinary Cooperation in the IGCP-Project 216 'Global Biological Events in Earth History' (ed. Walliser, O. H.) 35–51 (Springer, Berlin Heidelberg, 1996).
- Finnegan, S. et al. The magnitude and duration of Late Ordovician–Early Silurian glaciation. Science 331, 903–906 (2011).
- Brenchley, P. et al. High-resolution stable isotope stratigraphy of Upper Ordovician sequences: constraints on the timing of bioevents and environmental changes associated with mass extinction and glaciation. *Geol. Soc. Am. Bull.* 115, 89–104 (2003).
- 4. Sheehan, P. M. The Late Ordovician mass extinction. *Annu. Rev. Earth Planet. Sci. Lett.* **29**, 331–364 (2001).
- Yapp, C. J. & Poths, H. Ancient atmospheric CO<sub>2</sub> pressures inferred from natural goethites. *Nature* 355, 342 (1992).
- Berner, R. A. GEOCARBSULF: a combined model for Phanerozoic atmospheric O<sub>2</sub> and CO<sub>2</sub>. Geochim. Cosmochim. Acta 70, 5653–5664 (2006).
- Tobin, K. J., Bergström, S. M. & De La Garza, P. A mid-Caradocian (453 Ma) drawdown in atmospheric pCO<sub>2</sub> without ice sheet development? *Palaeogeogr. Palaeoclimatol. Palaeoecol.* 226, 187–204 (2005).
- Pancost, R. D. et al. Reconstructing Late Ordovician carbon cycle variations. Geochim. Cosmochim. Acta 105, 433–454 (2013).
- Kump, L. et al. A weathering hypothesis for glaciation at high atmospheric pCO<sub>2</sub> during the Late Ordovician. *Palaeogeogr. Palaeoclimatol. Palaeoecol.* 152, 173–187 (1999).
- 10. Buggisch, W. et al. Did intense volcanism trigger the first Late Ordovician icehouse? *Geology* **38**, 327–330 (2010).

 Melchin, M. J., Mitchell, C. E., Holmden, C. & Štorch, P. Environmental changes in the Late Ordovician–early Silurian: review and new insights from black shales and nitrogen isotopes. *Geol. Soc. Am. Bull.* 125, 1635–1670 (2013)

- Brenchley, P. et al. Bathymetric and isotopic evidence for a short-lived Late Ordovician glaciation in a greenhouse period. *Geology* 22, 295–298 (1994).
- Brenchley, P., Carden, G. & Marshall, J. Environmental changes associated with the 'first strike' of the Late Ordovician mass extinction. *Mod. Geol.* 20, 69–82 (1995).
- LaPorte, D. et al. Local and global perspectives on carbon and nitrogen cycling during the Hirnantian glaciation. *Palaeogeogr. Palaeoclimatol. Palaeoecol.* 276, 182–195 (2009).
- Luo, G. et al. Perturbation of the marine nitrogen cycle during the Late Ordovician glaciation and mass extinction. *Palaeogeogr. Palaeoclimatol. Palaeoecol.* 448, 339–348 (2016).
- Rohrssen, M., Love, G. D., Fischer, W., Finnegan, S. & Fike, D. A. Lipid biomarkers record fundamental changes in the microbial community structure of tropical seas during the Late Ordovician Hirnantian glaciation. *Geology* 41, 127–130 (2013).
- Newman, D. K., Neubauer, C., Ricci, J. N., Wu, C.-H. & Pearson, A. Cellular and molecular biological approaches to interpreting ancient biomarkers. *Annu. Rev. Earth Planet. Sci.* 44, 493–522 (2016).
- Higgins, M. B., Robinson, R. S., Husson, J. M., Carter, S. J. & Pearson, A. Dominant eukaryotic export production during ocean anoxic events reflects the importance of recycled NH<sub>4</sub>+. Proc. Natl Acad. Sci. USA 109, 2269–2274 (2012).
- Kaljo, D., Männik, P., Martma, T. & Nölvak, J. More about the Ordovician-Silurian transition beds at Mirny Creek, Omulev Mountains, NE Russia: carbon isotopes and conodonts Eston. J. Earth Sci. 61, 277–294 (2012).
- Finney, S. C. et al. Late Ordovician mass extinction: a new perspective from stratigraphic sections in central Nevada. Geology 27, 215–218 (1999).
- Finney, S. C., Berry, W. B. & Cooper, J. D. The influence of denitrifying seawater on graptolite extinction and diversification during the Hirnantian (latest Ordovician) mass extinction event. *Lethaia* 40, 281–291 (2007).
- Higgins, M. B. et al. Paleoenvironmental implications of taxonomic variation among δ<sup>15</sup>N values of chloropigments. *Geochim. Cosmochim. Acta* 75, 7351–7363 (2011).
- Sachs, J. P., Repeta, D. J. & Goericke, R. Nitrogen and carbon isotopic ratios of chlorophyll from marine phytoplankton. *Geochim. Cosmochim. Acta* 63, 1431–1441 (1999).
- Beaumont, V. I., Jahnke, L. L. & Des Marais, D. J. Nitrogen isotopic fractionation in the synthesis of photosynthetic pigments in *Rhodobacter* capsulatus and *Anabaena cylindrica*. Org. Geochem. 31, 1075–1085 (2000).
- Ahm, A.-S. C., Bjerrum, C. J. & Hammarlund, E. U. Disentangling the record of diagenesis, local redox conditions, and global seawater chemistry during the latest Ordovician glaciation. *Earth Planet. Sci. Lett.* 459, 145–156 (2017).
- French, K., Rocher, D., Zumberge, J. & Summons, R. Assessing the distribution of sedimentary C<sub>40</sub> carotenoids through time. *Geobiology* 13, 139–151 (2015).
- Junium, C. K., Freeman, K. H. & Arthur, M. A. Controls on the stratigraphic distribution and nitrogen isotopic composition of zinc, vanadyl and free base porphyrins through Oceanic Anoxic Event 2 at Demerara Rise. Org. Geochem. 80, 60–71 (2015).
- Delabroye, A. et al. Phytoplankton dynamics across the Ordovician/Silurian boundary at low palaeolatitudes: correlations with carbon isotopic and glacial events. *Palaeogeogr. Palaeoclimatol. Palaeoecol.* 312, 79–97 (2011).
- Lenton, T. M., Crouch, M., Johnson, M., Pires, N. & Dolan, L. First plants cooled the Ordovician. *Nat. Geosci.* 5, 86–89 (2012).
- Nodder, S. D. et al. Particle transformations and export flux during an in situ iron-stimulated algal bloom in the Southern Ocean. *Geophys. Res. Lett.* 28, 2409–2412 (2001).
- Kwon, E. Y., Primeau, F. & Sarmiento, J. L. The impact of remineralization depth on the air–sea carbon balance. *Nat. Geosci.* 2, 630–635 (2009).
- Lomas, M. et al. Increased ocean carbon export in the Sargasso Sea linked to climate variability is countered by its enhanced mesopelagic attenuation. *Biogeosciences* 7, 57–70 (2010).
- Bao, R. et al. Widespread dispersal and aging of organic carbon in shallow marginal seas. Geology 44, 791–794 (2016).
- 34. Hilligsøe, K. M. et al. Linking phytoplankton community size composition with temperature, plankton food web structure and sea-air CO<sub>2</sub> flux. Deep Sea Res. Part I: Oceanogr. Res. Pap. 58, 826–838 (2011).
- Michaels, A. F. & Silver, M. W. Primary production, sinking fluxes and the microbial food web. *Deep Sea Res. Part A: Oceanogr. Res. Pap.* 35, 473–490 (1988).
- Armstrong, H. A., Baldini, J., Challands, T. J., Gröcke, D. R. & Owen, A. W. Response of the inter-tropical convergence zone to Southern Hemisphere cooling during upper Ordovician glaciation. *Palaeogeogr. Palaeoclimatol. Palaeoecol.* 284, 227–236 (2009).

ARTICLES NATURE GEOSCIENCE

- Bjerrum, C. J., Bendtsen, J. & Legarth, J. J. F. Modeling organic carbon burial during sea level rise with reference to the Cretaceous. *Geochem. Geophys. Geosyst.* 7, Q05008 (2006).
- 38. Falkowski, P. G., Barber, R. T. & Smetacek, V. Biogeochemical controls and feedbacks on ocean primary production. *Science* **281**, 200–206 (1998).
- Bergman, N. M., Lenton, T. M. & Watson, A. J. COPSE: a new model of biogeochemical cycling over Phanerozoic time. *Am. J. Sci.* 304, 397–437 (2004).
- Pohl, A., Donnadieu, Y., Le Hir, G., Buoncristiani, J.-F. & Vennin, E. Effect of the Ordovician paleogeography on the (in)stability of the climate. *Clim. Past.* 10, 2053 (2014).
- 41. Chen, B. & Liu, H. Relationships between phytoplankton growth and cell size in surface oceans: interactive effects of temperature, nutrients, and grazing. *Limnol. Oceanogr.* **55**, 965–972 (2010).
- Fan, J., Peng, Pa & Melchin, M. Carbon isotopes and event stratigraphy near the Ordovician–Silurian boundary, Yichang, South China. *Palaeogeogr. Palaeoclimatol. Palaeoecol.* 276, 160–169 (2009).
- Holmden, C. et al. Nd isotope records of late Ordovician sea-level change implications for glaciation frequency and global stratigraphic correlation. *Palaeogeogr. Palaeoclimatol. Palaeoecol.* 386, 131–144 (2013).

## Acknowledgements

We gratefully acknowledge X. Wang (Johns Hopkins University) for valuable discussions on the execution and C++ code modification of the COPSE model. J.S. acknowledges financial support from Z. T. Guo and the China Scholarship Council. We thank D. T. Johnston and J. J. Kharbush for helpful discussions, and B. D. A. Naafs, S. J. Hurley and S. J. Carter for assistance with sample preparation and machine use. We thank

A. J. Kaufman for his help with bulk N-isotopic analysis of Vinini Creek samples. We thank D. Hu for the bulk N-isotope analysis of XY-5 samples. This study was supported by the National Natural Science Foundation of China (grant numbers 41520104007 and 41330102). A.P. received support from the NASA Astrobiology Institute and the Gordon and Betty Moore Foundation.

#### **Author contributions**

J.S. and A.P. designed the paper. J.S., G.A.H. and S.D.W. performed the biomarker analysis. J.S. and K.C. performed the bulk sediment analysis. J.S., A.P. and Y.G.Z. contributed to the data interpretation. D.L., S.C.F. and Y.S. collected the samples and provided a robust stratigraphic framework. J.S., A.P. and Y.G.Z. designed the biogeochemical model. J.S. wrote code and performed model simulations. J.S. and A.P. wrote the manuscript, with inputs from G.A.H., Y.G.Z., S.C.F. and S.D.W.

## **Competing interests**

The authors declare no competing interests.

#### Additional information

**Supplementary information** is available for this paper at https://doi.org/10.1038/s41561-018-0141-5.

Reprints and permissions information is available at www.nature.com/reprints.

Correspondence and requests for materials should be addressed to J.S. or A.P.

**Publisher's note:** Springer Nature remains neutral with regard to jurisdictional claims in published maps and institutional affiliations.

#### Methods

Materials. Samples were collected from the Vinini Creek section (Supplementary Fig. 5), Nevada, United States, which was deposited continuously in an intense upwelling zone in western Laurentia during the Late Ordovician<sup>44,45</sup>. The Vinini Creek section sediments were deposited in an off-platform to basinal environment<sup>40,21</sup> and contain four graptolite zones including *D. ornatus*, *P. pacificus*, *Metabolograptus extraordinarius* and *Metabolograptus persculptus*. The Vinini Creek succession has excellent biostratigraphic records of conodonts, graptolites and chitinozoans<sup>20</sup>. All 89 rock samples were collected from outcrops where fresh surface layers were exposed to avoid weathered or otherwise contaminated rock. Most samples were organic-rich, and 25 of the samples contained sufficient porphyrins in total lipid extracts for nitrogen isotopic analysis.

Sample preparation and isotopic analysis. Sample cleaning and extraction. All rock samples were sonicated in three solvents, including methanol (MeOH; Honeywell, GC230-4), dichloromethane (DCM; Honeywell, GC299-4) and hexane (Honeywell, GC215-4). The samples were broken into pebbles using a steel/chrome puck mill (CHRO-100-B; ROCKLABS Bench Top Ring Mill) in a ShatterBox (SPEX 8530), and the pebbles were again cleaned by all three solvents. Cleaned pebbles were crushed to a fine powder in the steel/chrome puck mill and the powder was collected into a combusted jar for storage. Samples were extracted using a MARS Microwave Reaction System (Model: MARS 230/60; Model number: 907501) in 9:1 DCM/MeOH at 100 °C to obtain total lipid extracts.

Porphyrin purification and collection. Porphyrin preparation followed a previously published method\*\*6. Total lipid extracts were separated using SiO $_2$ -gel chromatography with a 22 ml column (254 mm × 10.5 mm, Acc Glass PN#5888-10) to obtain four bulk fractions. Vanadyl (VO) porphyrins were eluted in Fraction 3 (F3) using 100% DCM. F3 was further purified using Normal phase (NP) high-performance liquid chromatography (HPLC, Agilent) on a ZORBAX SIL column (4.6×25 mm, 5  $\mu$ m) with an elution program (a 37 min gradient from 100% hexane to 100% ethyl acetate, at a 1 ml min $^{-1}$  flow rate). Absorbance was monitored at 405 nm for VO porphyrins; verification of VO porphyrin identity is shown in Supplementary Table 1. The entire VO porphyrin elution window was collected using an automated fraction collector. Each HPLC-purified porphyrin contained at least 50 nmol N. Vanadyl octaethylporphine (VO-OEP, Frontier Scientific) was used as the standard for both spectroscopic identification and nitrogen isotope composition\*\*6. Procedural blanks were used to confirm insignificant endogenous N contamination.

Nitrogen isotopic analysis. Porphyrin nitrogen isotopic analysis. HPLC-collected porphyrin fractions were oxidized to nitrate following a previously published two-step process\*: photooxidation under ultraviolet light in quartz tubes for 6 h in a Baker SterilGard III biological cabinet; followed by reaction with recrystallized persulfate oxidizing reagent ( $K_2 S_2 O_8/NaOH, 0.05\,mM$  and  $0.15\,mM$ , respectively) in an autoclave for 30 min at  $121\,^{\circ}C$ . Nitrate concentration and nitrogen isotopic composition were analysed at Woods Hole Oceanographic Institution. Nitrate concentration was measured by chemiluminescent detection of NO after conversion in a hot solution of V(III) (ref.  $^{47}$ ). Samples containing at least  $\sim \! 10\, \text{mol N}$  were measured for nitrogen isotopic composition by the denitrifier method  $^{48}$ , with a precision of generally < 0.3%. Selected samples were replicated through the entire process—authentic complete replication of the data starting with initial rock powders.

<u>Bulk nitrogen isotopic analysis</u>. Bulk sedimentary nitrogen isotopic values ( $\delta^{15}N_{TN}$ ) were analysed on a Thermo-Finnigan MAT 253 isotope ratio mass spectrometer coupled with the Thermo Scientific Flash HT Plus elemental analyser using USG\$40 as a standard. All bulk nitrogen isotope analyses were measured at the University of Science and Technology of China. All data are reported using standard  $\delta$  notation relative to atmospheric  $N_2$ . Standard precision is better than 0.25% and triplicate measurements of selected samples are 0.25%.

Nitrogen isotope values of bulk sediment. All bulk elemental content and isotopic data presented herein are new (Supplementary Table 2). The base of the M. extraordinarius graptolite zone is the start of the Hirnantian stage, which is accompanied by the onset of the  $\delta^{13}C_{\rm org}$  positive excursion. Our  $\delta^{16}C_{\rm org}$  and  $\delta^{15}N_{\rm TN}$  profiles are well correlated with other Late Ordovician records  $^{1,14,1,15}$  (Supplementary Fig. 1), as similar ranges and temporal patterns of  $\delta^{15}N$  profiles exist in coeval sections (mean excursion of  $1.6\pm0.7\%$ ,, with average maximum  $\delta^{15}N_{\rm TN}$  value of 2.3%). Lack of correlation between TOC, TN and  $\delta^{15}N_{\rm TN}$  indicate that  $\delta^{15}N_{\rm TN}$  trends are not dependent on organic carbon concentrations (Supplementary Figs. 3 and 4). Thus, it is unlikely that our bulk isotopic records have been extensively thermally altered prior to burial.

Consideration of porphyrin diagenesis. Interpretation of our bulk sediment  $(\delta^{19}N_{TN})$  and porphyrin nitrogen isotope data depends on understanding how porphyrin diagenesis affects the magnitude of  $\epsilon_{por}$ . For Vinini Creek,  $\epsilon_{por}$  applies specifically to VO porphyrins, because the other major porphyrin types either were not assessed (free base porphyrins, FB), or were assessed but found to be in low concentration (zinc porphyrins, Zn). Junium et al.  $^{27}$  proposed that porphyrin  $\delta^{19}N$  values become isotopically fractionated during sequential diagenesis of chlorophyll

 $\rightarrow$  free base (FB)  $\rightarrow$  Zn  $\rightarrow$  VO porphyrins. The fractional distribution of final products, plus the values of  $\epsilon_{Zn}$  and  $\epsilon_{VO}$ , therefore determine the final  $\delta^{15}N$  values of the individual porphyrin pools.

The allowed isotope space for diagenetic porphyrins under any scenario is governed by the following equations (derived from relationships in ref. 49).

$$\begin{split} \varepsilon_{\mathrm{VO}} &= \delta_{\mathrm{Zn}} - \delta_{\mathrm{VO}} \\ \varepsilon_{\mathrm{Zn}} &= \delta_{\mathrm{FB}} - \frac{(\delta_{\mathrm{TotPor}} - f_{\mathrm{FB}} \delta_{\mathrm{FB}})}{(1 - f_{\mathrm{FB}})} \\ 1 &= f_{\mathrm{FB}} + f_{\mathrm{Zn}} + f_{\mathrm{VO}} \end{split}$$

At values of  $\epsilon_{Zn}$  and  $\epsilon_{VO}$  consistent with the experiments and data of Junium et al.  $^{27}$ , the solutions to these equations require that VO porphyrins have the most negative  $\delta^{15}N$  values ( $\delta_{VO} < \delta_{FB}$  and  $\delta_{Zn}$ ). More importantly, it is possible to have a diverse range of values of  $\delta_{VO}$  under conditions of  $\epsilon_{por} = 5\%$  (which is the proposed endmember for 100% eukaryotic export production in refs  $^{18,22}$ ).

Viewed in this context, the scatter in values for VO porphyrins from Vinini Creek probably reflects a combination of genuine heterogeneity of porphyrin sources and diagenetic fates, compounded with analytical error. Adopting values of  $\epsilon_{\rm Zn}$  and  $\epsilon_{\rm VO}$  implied by ref.  $^{\rm 27}$ , a maximum estimate of 10% Zn porphyrins for our samples (qualitatively, they contained VO  $\gg$  Zn porphyrins), an average value of  $\delta_{\rm VO}$  = -6.3%, we find that approximately all diagenetic yields of > 35% FB porphyrins will yield values of  $\delta_{\rm VO}$  < -6% (and can be below -8% at > 80% FB porphyrins).

Organic burial flux database. Organic-rich late Katian shales are found in a wide range of depositional settings. The prevalence of this lithofacies appears to indicate relatively hypoxic to anoxic ocean conditions and high levels of organic carbon sequestration associated with a strong transgression<sup>45,50,51</sup>. Although Melchin et al.<sup>11</sup> made a thorough and global compilation of the distribution of black shales during the Ordovician–Silurian transition, to date there is no quantitative assessment of how much the organic carbon burial flux actually changes during this time.

For this study, we set up an organic carbon burial flux database to quantitatively investigate the expansion of burial flux during the late Katian. This database is sorted into three specific time intervals: two preceding (*D. ornatus*, *P. pacificus*) and one during the Hirnantian glaciation. The data include profile records from different palaeo-continental regions (Supplementary Fig. 5). We compiled published data including sample depth, timescale, rock density, and total organic carbon (TOC) concentrations, and then determined burial flux by calculating the TOC accumulation rate:

Organic Carbon Burial Flux(g m<sup>-2</sup> per 
$$10^6$$
 yr) =  $\frac{z}{\Delta t} \times \rho \times \%$ TOC (1)

where z is thickness,  $\Delta t$  is the time interval and  $\rho$  is density. Supplementary Table 3 shows the burial flux results, localities, data sources and a data quality assessment. Due to lack of good age control, our calculated burial flux is especially uncertain for the late Katian D. ornatus stage. To minimize this uncertainty, we utilized the known sedimentation rates of the P. pacificus stage and the Hirnantian interval to get maximum and minimum estimates of burial flux for the D. ornatus stage, as well as an average value. Records assessed as 'poor' by our quality criteria (biostratigraphy, hiatus and %TOC data) were discarded before the calculations.

Expanded organic carbon burial appears to be widespread during the P. pacificus stage of the late Katian, occurring in five of the seven localities (Supplementary Fig. 6). When the average across all regions is normalized to the D. ornatus zone (including average, max and min values), burial flux appears to have been higher by a factor of 3.9 (min: 3.2 and max: 4.4) during the P. pacificus stage and by a factor of 1.8 (min: 1.6 and max: 2.0) during the Hirnantian. If normalized to the Hirnantian interval, burial flux during the P. pacificus stage appears to have been higher by a factor of 2.1. Hence, these results demonstrate that there was a maximum in organic carbon burial flux in P. pacificus, prior to the onset of glaciation. Although the reported sections are strongly biased by continental shelf sites, 80% of global marine organic matter is accumulated on continental shelves<sup>52</sup>, so the data are believed to be representative of conditions during the Late Ordovician. Similarly, although the magnitude of the estimated burial flux increase is influenced strongly by the high TOC content of the Vinini Creek section, the section may be representative of other, similar, burial environments; and the general phenomenon of increased carbon burial is seen at most sites, not only at Vinini Creek. Therefore we believe that this databasealthough containing relatively few sections—provides a reasonable assessment of organic burial flux changes during the Late Ordovician and is suitable for constraining model input scenarios.

**Modelling.** The COPSE model is presented in ref. <sup>39</sup>, which can be run with a resolution of 1 Myr. Here we modified it by two separate approaches, and then we compared those two approaches.

First, we directly modified the value of marine organic carbon burial (*mocb*) according to changes in burial flux prescribed by Supplementary Table 3. We call this version 'direct burial forcing'. Second, we removed the prescribed direct burial

ARTICLES NATURE GEOSCIENCE

forcing and instead changed *mocb* to be a function of three variables: phosphorus, phytoplankton community structure, and sea level. We call this version 'community and environmental parameters'. Details of these implementations are described below.

COPSE Model: Direct burial forcing. Model adaption. In order to examine the CO<sub>2</sub> draw-down caused by increased marine organic carbon burial during the late Katian, marine organic carbon burial was controlled using an external forcing parameter (called JH). The value of JH was prescribed based on the flux database results (Supplementary Table 3). Parameter JH was used to scale the value of marine organic carbon burial (mocb) at ~447 Ma. Specifically, JH = 1 until 447 Ma, then rises to 3.9 at 445 Ma, drops to 1.8 at 444 Ma, and declines to 1 at 442 Ma (Fig. 2, green lines). For the upper error limit, JH = 1 up to 447 Ma, then rises to 3.2 at 445 Ma, drops to 1.6 at 444 Ma, and declines to 1 at 442 Ma (Fig. 2, upper limit of shaded grey areas). For the lower error limit, JH = 1 up to 447 Ma, then rises to 4.4 at 445 Ma, drops to 2.0 at 444 Ma, and declines to 1 at 442 Ma (Fig. 2, lower limit of shaded grey areas).

<u>Choice of initial conditions</u>. The model was initiated using background conditions to simulate  $\mathrm{CO}_2$  and temperature before invoking any changes in *mocb*. The results are therefore sensitive to the model's geological forcing factors (degassing, D; uplift, U), as described in refs <sup>29,39</sup>. We then varied D and U over 1.2–1.8 and 1.2–0.8, respectively, to find lower and upper limits for the  $\mathrm{CO}_2$  and temperature scenarios when *mocb* is forced by JH (Supplementary Fig. 7).

The results suggest an upper scenario for the evolution of Late Ordovician atmospheric CO<sub>2</sub> of 11.3 PAL at 450 Ma, reduced to 7.8 PAL at 444 Ma (Supplementary Fig. 7, orange dashed lines). The lower scenario suggests an initial CO<sub>2</sub> value of 5.5 PAL at 450 Ma, reduced to 1.9 PAL at 444 Ma (Supplementary Fig. 7, purple dashed lines). We chose a consensus estimate for these parameters that yields a global temperature of 17 °C and an atmospheric CO<sub>2</sub> of 8 PAL at 450 Ma to initiate the model (Supplementary Fig. 7, green solid line); our final parameter choices for initial conditions are thus the same as ref. <sup>29</sup> (D = 1.5 and U = 1). A CO<sub>2</sub> concentration in this range is consistent with previous proxy constraints<sup>7,8</sup>.

COPSE Model: Substitution of community and environmental parameters. <u>Model adaptation</u>. Two new external forcing parameters–phytoplankton community structure and sea-level change–were introduced into the COPSE model, combining them with the phosphorus forcing as implemented by ref.<sup>29</sup> in order to examine how the marine organic carbon burial (*mocb*) amplification was promoted. We made the following three changes.

- Phosphorus weathering (F) was included as a normalized forcing parameter as
  proposed in ref. <sup>29</sup>.
- Phytoplankton community structure (Ag) was introduced as a forcing parameter scaled between 0 and 1 to indicate the proportion of eukaryotes. The values prescribed for this forcing are calculated from our porphyrin biomarker results  $(\epsilon_{\mbox{\tiny por}})\!,$  which allow prediction of the fraction of the population that is eukaryotic. The lipid biomarker stratigraphic records only span from just before 446.5 to 444 Ma, which means we are only able to get three "known" Ag values: at 446 Ma (the base of P. pacificus zone), 445 Ma (uppermost part of the P. pacificus zone) and 444 Ma (uppermost part of the P. persculptus zone). Thus, Ag values for these times are 0.6, 1 and 0.8, respectively (Supplementary Figs 9 and 10). A variable to modify the burial efficiency of these eukaryotes, denoted as kk\_Ag, was also included to represent the organic carbon burial efficiency by eukaryotes, in order to differentiate large and small cells, using the principle that larger cells will have faster sinking and therefore more efficient carbon removal from the surface. The proposed kk\_Ag has a larger value than kk2 (burial efficiency in the original COPSE Model<sup>39</sup>). Hence, the new mocb flux function (Eq. 2) contains two terms in which different phytoplankton burial efficiencies are assigned to the two components of biomass, an average "small" biomass community with presumed slow sinking rates (kk2) and an average "large" biomass community with high sinking rates (kk\_Ag). The time-evolving quantity of carbon partitioned between the two terms Ag and (1-Ag) is prescribed by the  $\epsilon_{\mbox{\tiny por}}$  results. These variables were used instead of the monotonic organic carbon burial efficiency that was prescribed in the original COPSE model.
- Sea-level forcing (SI) was introduced as a flag parameter to indicate when
  more marine organic carbon burial (denoted by a constant, α) was promoted
  due to the rise of sea level (marine transgression).

With these modifications, the new mocb flux function was expressed as follows, and used instead of equation (30) in ref.  $^{39}$ .

$$mocb = (1 - Ag) \times kk2 \times (newp')^2 + Ag \times kk Ag \times (newp')^2 + Sl \times \alpha$$
 (2)

where kk2 is the export efficiency of cyanobacteria, and newp' means the normalized oceanic new production. We ran the model with the following parameter variations (Fig. 2, orange lines).

Set 1: F = 1 until 446 Ma, increase to F = 2.2 between 446 Ma and 445 Ma, then linear decline to F = 1 at 443 Ma, constant thereafter.

Set 2: Sl = 1 between 446 Ma and 445 Ma, otherwise Sl = 0.

Set 3: Ag=0 until 446 Ma, increase to Ag=0.6 between 446 Ma and 445 Ma, increase to Ag=1.0 between 445 Ma and 444 Ma, then drop to Ag=0.8 between 444 Ma and 443 Ma, and linear decrease to 0 at 442 Ma, constant thereafter (Supplementary Fig. 10).

Sensitivity analysis. We examined the sensitivity of the model results to the values assigned to phosphorus weathering (F), increased sea level (S), and phytoplankton export efficiency ( $kk\_Ag$ ). The values of the Ag forcing were not adjusted, as they are assigned based on our porphyrin biomarker results ( $\epsilon_{por}$ ). All sensitivity analyses and results are summarized in Supplementary Table 4(A-C) and 5, and Supplementary Fig. 8.

Step 1: Sensitivity to phosphorus weathering (F)

To reproduce the Hirnantian carbon isotope excursion (HICE), a temporary tripling of global phosphorus weathering was required in the ref. 29 modification of the COPSE Model. Lenton et al.29 hypothesized that this increased pulse of phosphorus weathering might have been enabled by the colonization of the first terrestrial vascular plants. Their simulations required temporary amplification of the phosphorus weathering parameter (F) by a factor of three at  $\sim$ 445 Ma, causing CO<sub>2</sub> to reduce to 4.5 PAL. Although the magnitude and timing of this phosphorus pulse is somewhat uncertain because of the uncertainty of the HICE magnitude and the presumably small total size and activity of the early terrestrial plant biota during the Late Ordovician, evidence from the sedimentary record does show increased phosphorus deposition at around 500 Ma (ref. 53). However, we found that the magnitude of F could be reduced in our revised model. Reduction of F to a uniform value of two (instead of three in ref. 29) partially achieves the required CO<sub>2</sub> decrease (Supplementary Table 4(A), step 1.1), but a small adjustment of both the timing of maximum phosphorus weathering to ~446 Ma (instead of 445 Ma) and to a magnitude of F = 2.2 shows better alignment with the peak of organic carbon burial (Supplementary Table 4(A), step 1.2). The resulting atmospheric CO<sub>2</sub> and temperature trends are shown in Supplementary Fig. 8 (step 1.1 and step 1.2).

Step 2: Sensitivity to sea-level increase (Sl)

Pre-Hirnantian sea levels were among the highest stands in geological history. Large-scale transgression occurred in the late Katian <sup>11,36,34</sup>, which created an environment that had more accommodation space for sediment accumulation and organic carbon burial. Although the magnitude of this increase is not well understood for the Late Ordovician, a similar (or slightly smaller) sea-level rise during the Cretaceous was estimated to increase organic carbon burial by 30% (ref. <sup>37</sup>). Here we accounted for this transgression by introducing a flag parameter forcing (SI) to indicate when more mocb was enhanced; we assumed the increase was 30% compared to baseline mocb, although it may have been larger. We kept the values of F from Step 1.2, where F=2.2 at ~446 Ma, F=1.8 at ~445 Ma and F=1.4 at ~444 Ma. And furthermore, since we focus on the time immediately preceding and during the Hirnantian period, SI was increased between 446 Ma and 445 Ma, in the late Katian (Supplementary Table 4(B), step 2). The resulting atmospheric  $CO_2$  and temperature trends are shown in Supplementary Fig. 8 (step 2).

Step 3: Sensitivity to phytoplankton export efficiency  $(kk\_Ag)$ 

Plankton community structure can influence organic carbon burial due to different cell size, density and transfer behaviour  $^{12,35,55,56}$ . Our porphyrin biomarker results suggest that around  $\sim$ 20% eukaryotic biomass in the *D. ornatus zone* gradually expanded and then reached nearly 100% in the uppermost *P. pacificus zone* (Supplementary Fig. 9). This indicates the expansion of large-sized eukaryotes having high export efficiency, before the onset of Hirnantian glaciation. Here we explore the change in burial efficiency caused by increased size of eukaryotic algae using a parameter for sinking efficiency ( $kk\_Ag$ ).

To achieve the agreement with the direct burial forcing scenario—that is, with the sediment flux database (Fig. 2 green lines)—we examined the relationship between  $kk\_Ag$  and kk2 with five different runs for sensitivity analyses. In each run,  $kk\_Ag$  is one to five times higher than kk2, respectively, while keeping F and Sl unchanged compared to Step 2, where F=2.2, Sl=1 at  $\sim$ 446 Ma, F=1.8, Sl=0 at  $\sim$ 445 Ma, F=1.4, Sl=0 at  $\sim$ 444 Ma. The resulting CO<sub>2</sub> and temperature trends are shown in Supplementary Fig. 8 (step 3.1–step 3.5, step 3.1 is similar to step 2 since  $kk\_Ag=kk2$ ).

Step 4: Summary

Based on the sensitivity analyses above, we found that the best simulation (Fig. 2, orange lines) to achieve the same carbon burial as the directly observed mocb (Fig. 2, green lines) is when the marine burial efficiency of eukaryotes is increased by a factor of four  $(kk\_Ag=4\times kk2)$  (Supplementary Table 5). According to Stokes' Law, fourfold export efficiency is expected from a doubling in cell size. In this best solution, phosphorus weathering is amplified by a factor of approximately two and burial is increased by 30% due to the transgression as noted above. Our results therefore support the idea that these three parameters can work synergistically to play important roles in the expansion of organic burial flux and rapid decrease in atmospheric  $\mathrm{CO}_2$ . Although the fine-scale temporal

complexity of the marine carbon cycle is not well captured by the COPSE model, our model simulation helps clarify how rates of carbon burial could be associated with broad changes in phytoplankton community structure and how this may change in tandem with (or nonlinearly with) changes in nutrient loading. Future work must focus on constraining the burial efficiency of different phytoplankton groups to rigorously clarify the links between community succession and carbon burial in the geologic reservoir.

**Code availability.** The code used to perform COPSE simulations can be accessed at https://figshare.com/s/8b7830d6ef1cbde44428.

**Data availability.** The authors declare that data supporting the findings of this study are available within the article and its Supplementary Information files. Complied data derive from previously published studies (see reference lists).

## References

- 44. Wilde, P. in *Advances in Ordovician Geology* Paper 90-9 (eds Barnes, C. R. & Williams, S. H.) 283–298 (Geological Survey of Canada, Ottawa, 1991).
- Berry, W. B. Black shales: An Ordovician perspective. Geol. Soc. Am. Spec. Pap. 466, 141–147 (2010).
- Higgins, M. B., Robinson, R. S., Casciotti, K. L., McIlvin, M. R. & Pearson, A. A method for determining the nitrogen isotopic composition of porphyrins. *Anal. Chem.* 81, 184–192 (2009).

 Braman, R. S. & Hendrix, S. A. Nanogram nitrite and nitrate determination in environmental and biological materials by vanadium (III) reduction with chemiluminescence detection. *Anal. Chem.* 61, 2715–2718 (1989).

- 48. Sigman, D. et al. A bacterial method for the nitrogen isotopic analysis of nitrate in seawater and freshwater. *Anal. Chem.* **73**, 4145–4153 (2001).
- 49. Hayes, J. M. Fractionation of carbon and hydrogen isotopes in biosynthetic processes. *Rev. Mineral. Geochem.* 43, 225–277 (2001).
- Berry, W. B. & Wilde, P. Progressive ventilation of the oceans; an explanation for the distribution of the lower Paleozoic black shales. *Am. J. Sci.* 278, 257–275 (1978).
- Leggett, J. British Lower Palaeozoic black shales and their palaeooceanographic significance. J. Geol. Soc. 137, 139–156 (1980).
- Berner, R. A. The Phanerozoic Carbon Cycle: CO<sub>2</sub> and O<sub>2</sub> (Oxford Univ. Press, Oxford, 2004).
- Reinhard, C. T. et al. Evolution of the global phosphorus cycle. Nature 541, 386–389 (2017).
- Haq, B. U. & Schutter, S. R. A chronology of Paleozoic sea-level changes. Science 322, 64–68 (2008).
- Klaas, C. & Archer, D. E. Association of sinking organic matter with various types of mineral ballast in the deep sea: implications for the rain ratio. *Global Biogeochem. Cycles* 16, 1116 (2002).
- Kostadinov, T., Siegel, D. & Maritorena, S. Global variability of phytoplankton functional types from space: assessment via the particle size distribution. *Biogeosciences* 7, 3239–3257 (2010).